Frontiers of Architectural Research 15 (2026) 1572—1588

Available online at www.sciencedirect.com

ScienceDirect

journal homepage: www.keaipublishing.com/foar

RESEARCH ARTICLE

Introducing a Perceptual—Spatial Landscape Planning Model (PSLPM) for cultural landscapes' route optimization: The case of Chengde Mountain Resort

Jingsen Lian*, Steffen Nijhuis, Gregory Bracken, Nan Bai, Haoxiang Zhang

Delft University of Technology, Delft 2614HT, Netherlands

Received 17 June 2025; received in revised form 23 October 2025; accepted 23 October 2025

KEYWORDS
Cultural landscape planning;
Perceptual-spatial coupling;
Large language model;
Graph neural networks;
Multi-objective evolutionary algorithm;
Route optimization

Abstract As cultural landscapes increasingly evolve within urban environments, a persistent gap has emerged between their heritage spatial characteristics and public heritage value perception, undermining urban identity and sustainability. This study introduces the Perceptual—Spatial Landscape Planning Model, an integrative framework that positions route optimization as a strategic planning intervention to bridge this gap. Taking Chengde Mountain Resort as a case, we constructed a spatial network of 144 scenes and collected 43,879 user-generated social media comments to quantify public perception. We achieved perceptual—spatial coupling through: 1) a few-shot learning paradigm based on a large language model generates five distinct perception scores of each scene; 2) the resulting scores are then integrated with heritage spatial characteristics in graph neural networks using graph attention networks and deep graph infomax. Based on the coupling process, the optimized routes were generated by a multi-objective evolutionary algorithm. The optimized routes outperformed official and greedy baselines, achieving higher spatial diversity, perceptual coherence, lower variance, and broader coverage of marginal yet meaningful scenes. These routes avoided over-concentration in perceptual hotspots as conventional tourism planning while enhancing interpretive richness across various spaces. This model provides strong contextual transferability, offering interpretable framework for integrating public perception into cultural landscape planning, thereby advancing both the methodological rigor and spatial intelligence of cultural landscapes' development in urban environments.

* Corresponding author.
E-mail address: J.s.Lian@tudelft.nl (J. Lian).
Peer review under the responsibility of Southeast University.

https://doi.org/10.1016/j.foar.2025.10.004

1. Introduction

Cultural landscapes are increasingly recognized as dynamic spaces shaped by human perception, identity, experience, and meaning (Sahle and Saito, 2021; Singh et al., 2023). As urbanization accelerates, an increasing number of cultural landscapes integrated into urban environments are facing significant challenges (Bornioli et al., 2023; Liu et al., 2022): an apparent mismatch between heritage spatial characteristics (HSCs) and public heritage value perception (PHVP). This mismatch renders cultural landscapes vulnerable to marginalization during the urban renewal process, where pressures from tourism development, planning inertia, or commercial logic often lead to a dilution of their contextual meaning, thereby eroding their values and characteristics (Tena et al., 2024). This erosion weakens public awareness and emotional connection to the cultural landscape, undermines sustainability, and leads to the loss of urban identity and cultural continuity (Soyer and Tunca, 2025).

To address this, a mediating mechanism is needed to link HSCs with PHVP. Route optimization can serve as such a bridge between cultural landscapes, the city, and the public, functioning as a perception-oriented medium that transcends the limitations of purely physical-spatial connectivity (Liang et al., 2024). The spatial complexity of many cultural landscapes does not always correspond to their heritage value perception (e.g., secluded palaces vs. open squares); yet, route optimization offers the potential to reconcile spatial connectivity with perceptual sequencing without compromising the underlying cultural logic (Öztürk and Aktan, 2024; Ryan, 2020). As debates over the conservation and development of cultural landscapes intensify, route optimization offers a strategic intervention to balance conservation policy with contemporary urban demands (Smith, 2023). It can mitigate congestion, relieve tourism pressure, and redistribute value across space, enabling visitors to engage with the cultural landscape in a sequential, value-driven manner aligned with public interest (Lin et al., 2024).

1.1. The perceptual—spatial gap of cultural landscapes' route optimization

A critical research gap remains in cultural landscapes' route optimization: The disconnection between HSCs and PHVP. On the one hand, existing studies have emphasized the identification of objective spatial structural features, but few have conducted in-depth analyses of how these spatial factors influence PHVP. Previous studies have focused more on the impact of spatial visibility, movement patterns, transition probabilities, accessibility, connectivity, and specific points of interest on tourist behaviour (Jamhawi et al., 2023; Zhang et al., 2023). However, overemphasis on objective spatial factors while neglecting users' subjective preferences (Liu et al., 2022) has led to suboptimal value alignment in tour routes and unsatisfactory user experiences (Liang et al., 2024; Vansteenwegen et al., 2010). On the other hand, some studies have explored the integration of various AI techniques to analyze public perception with user-generated content, revealing the potential of social media data (Bai et al., 2023) to capture comprehensive perceptions of heritage (Ai et al., 2024; B. Wang et al., 2024; Xu et al., 2024), but these applications have mainly focused on textual understanding, narrative generation, and personalized interaction, without integrating such insights into spatial-practical route optimization (Trichopoulos, 2023). They focus more on functional tool-oriented development (Wong et al., 2023), with limited efforts toward jointly holistic modeling and quantitatively identifying the relationship between cultural landscapes' HSCs and PHVP. As a result, route optimization lacks multi-dimensional perceptual alignment, which needs more precision and perceptual-spatial relevance (Liang et al., 2024).

1.2. A Perceptual—Spatial Landscape Planning Model

As an integrative approach that combines spatial organization with the communication of value perception, landscape planning fundamentally aims to facilitate the transformation of place-based cultural meanings through spatial configuration (Lian et al., 2024; Ryan, 2011; Sánchez et al., 2020). In a cultural landscape, spatial forms are not neutral containers but carriers of embedded narratives, historical references, and symbolic meanings (Henning et al., 2021; Von Haaren, 2002). Landscape planning as an approach draws upon this spatial characteristic to align physical structures with intangible heritage value perception of the public (Ducci et al., 2023), transforming landscape into a medium of cultural communication (Bohnet et al., 2022).

In this study, the proposed Perceptual-Spatial Landscape Planning Model (PSLPM) is grounded in the core logic of landscape planning. PSLPM employs spatial indicators to delineate landscape structure, while simultaneously incorporating public perception to establish a route optimization mechanism. Specifically, PSLPM combines few-shot learning from large language models to extract multidimensional heritage value perception, graph neural networks to embed perceptual-spatial complexity, and a multi-objective evolutionary algorithm to generate optimized routes that balance spatial diversity with perceptual coherence. Rather than offering a purely technical solution, PSLPM contributes to a strategic framework that embodies planning principles and addresses issues of spatial management and sustainability, extending beyond the enhancement of tourist experiences to include the broader goal of improving the perceptual quality. By bridging theoretical principles with AI-driven input, PSLAPM advances communicative efficacy of cultural landscapes through practical planning interventions.

2. Method

2.1. The framework of PSLPM

The framework of PSLPM is illustrated in Fig. 1. This diagram illustrates a streamlined framework for optimizing cultural landscape routes based on public perception and spatial features. Social media comments (43,879) are scored by LLMs into five PHVP categories. GIS-based analysis generates two HSC layers, integrated through principal component analysis (PCA). A Graph Neural Network (GNN) with Deep Graph Infomax learns 32D spatial embeddings. These data are coupled and optimized using a Multi-Objective Evolutionary Algorithm (NSGA-II) to generate five routes. Two baseline methods (greedy algorithm and official routes) are included for comparison. Final analyses assess PHVP and HSC differences across routes.

2.2. Study area

This study analyzes the Chengde Mountain Resort (CMR) as a typical cultural landscape case for other universal applications. CMR was inscribed on the UNESCO World Heritage List in 1994. It embodies a distinctive spatial expression of the Chinese national civilization's understanding of landscape order and cosmology. Integrating political, religious, ecological, and aesthetic values, CMR represents a concentrated manifestation of the Eastern philosophical concept of harmony between humans and nature. Its heritage significance is not only tied to national historical memory and identity but also offers the international community a unique perspective on Chinese culture (UNESCO, 1994).

Built in 1703 in Hebei province, China (Fig. 2), the CMR (5.64 km^2) comprises many smaller scenes, which reflect the historic scenic spots like other cultural landscapes, including fantastic views, buildings, courtyards, rockeries, waterscapes, and vegetation. We based our study on 144 representative scenes (named and numbered by the emperors who designed CMR). These scenes are not isolated visual fragments but are interconnected through a carefully landscape planning that guides movement, frames visual relationships, and layouts experiential rhythm. Spatial design techniques such as axial alignment, courtyard enclosure, and collective scenery shape a layered spatial sequence within the CMR, while simultaneously evoking multiple perceptual experiences, including cultural symbolism, religious connotation, and poetic or artistic imagination.

This interaction between spatial structure and perceptual meaning reflects a dual logic universal to many other cultural landscapes: it functions both as a mechanism for physical landscape planning order and as a medium for cultural expression. In the specific context of the CMR, such a spatial—perceptual coupling embodies cultural ideals and aesthetics, while also contributing to a historically grounded model of landscape construction that holds broad significance for heritage perception.

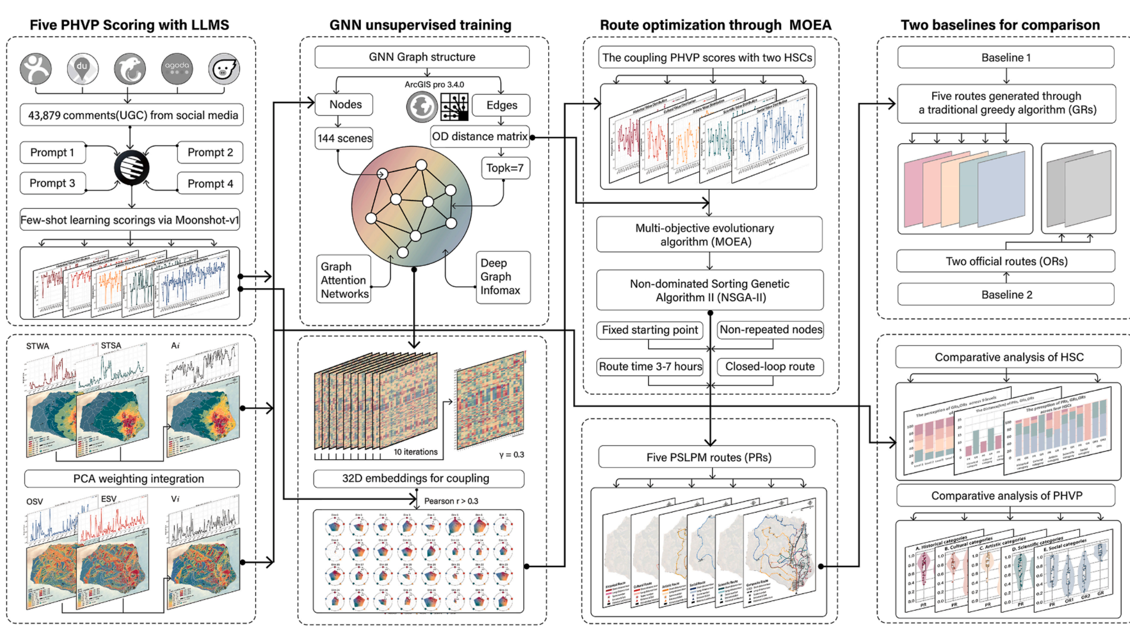

Fig. 1 The framework of PSLPM route optimization.

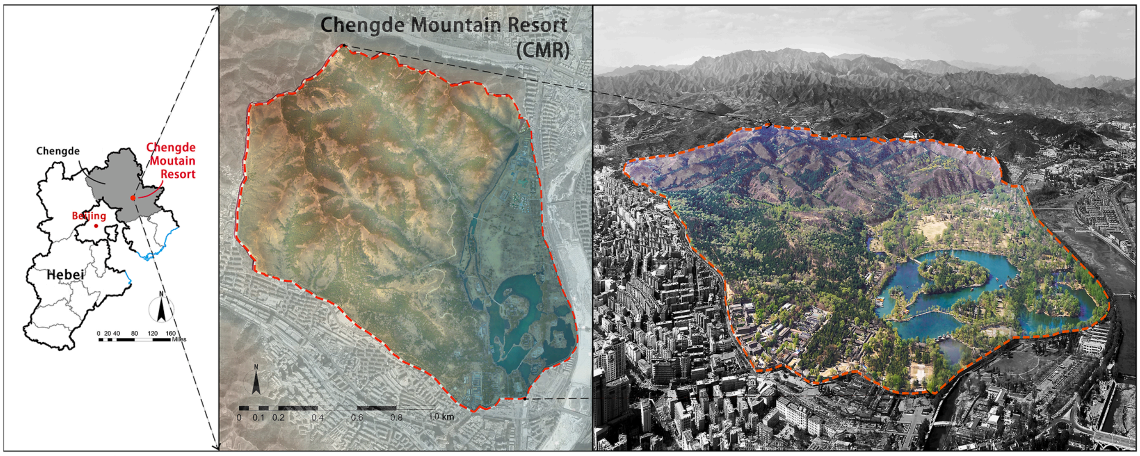

Fig. 2 The location and the aerial photography of Chengde Mountain Resort.

2.3. Data collection

All data used in this study were classified into two categories: (1) cultural landscape spatial data, employed to characterize the spatial attributes of the CMR; and (2) user-generated content from social media platforms, used to identify public perceptions of heritage values (Table 1).

The selected platforms represent different user communities and functions. Dianping focuses on attraction reviews, Ctrip, Fliggy, and Agoda emphasizes itinerary sharing and user ratings, while Baidu Maps provides mapping-based spatial tagging. This combination ensures comprehensive and diversified perception coverage. To ensure data quality and heritage relevance, a two-step filtering protocol was applied: (1) only comments that explicitly referenced one or more of the 144 scenes were retained; (2) exact duplicates were identified and removed based on SHA-256 hash comparisons and near-duplicate content was filtered using sentence-level BERT embeddings with a cosine similarity threshold of 0.95. This ensured that retained comments were both unique and semantically relevant to specific cultural scenes. After filtering, a total of 43,879 unique and scene-relevant comments were retained.

2.4. Data analysis

2.4.1. Cultural landscape spatial data analysis

The spatial characterization of the CMR is closely related to two key indicators: accessibility and visibility. These two indicators not only reflect the functional organization of the site but also embody its cultural, symbolic, and experiential significance:

Accessibility can be further divided into Scene-to-Water Accessibility (STWA) and Scene-to-Scene Accessibility (STSA). STWA was included to capture the proximity of scenes to water bodies of CMR. Water is recognized as a typical compositional element that plays a critical spatial and symbolic role in many cultural landscapes, shaping a

Table 1 The two categories of data.

Data category	Type/format	Capture tools	Data source
Cultural landscape spatial data	3D cloud points (.las format) 0.5 m digital surface models (DSMs) including vegetation	Matrice 300 Real Time Kinematic equipped with a DG4 Pro penta-lens camera Agisoft PhotoScan Pro vl.3.0.3772 and Agisoft Metashape Pro v1.7.4.12950	Close-range photogrammetry conducted by the Chengde Cultural Heritage Bureau
User-generated content from social media data	From an initial total of 59,852 comments, 43,879 were retained after filtering.	These data span a ten-year period from January 2015 to March 2025 and were retrieved through publicly accessible interfaces using a keyword-based search strategy. Specifically, we employed the official names, aliases, and spatial identifiers of the 144 predefined scenes in the CMR as query terms. The distribution of comments across platforms was as follows: Dianping (20,367), Ctrip (13,918), Fliggy (8,633), Baidu Maps (11,057), and Agoda (5,877).	Dianping, Ctrip, Fliggy, Baidu Maps, and Agoda

scene's aesthetic, ecological, recreational, and symbolic functions. (Balcan et al., 2024; Wallach, 2005; Zhang and Taylor, 2020). STSA, on the other hand, reflects the degree of movement and spatial connectivity among different scenes. It relates to the narrative and experiential continuity of the landscape, as evidenced by spatial autocorrelation patterns, and plays a key role in shaping spatial perceptions and cultural engagement across the site (Liao and Liang, 2025; Wu and Chen, 2022). Visibility can be further divided into Observed Scene Visibility (OSV) and Exterior Scene Visibility (ESV). OSV measures how frequently a scene is encountered along visitor routes, thereby indicating its visual exposure and spatial privacy. This passive visual perception dimension is essential for understanding how often and from where a scene contributes to the overall experiential structure (Domingo et al., 2020; Kim et al., 2020). ESV quantifies the visual openness of a scene's exterior, reflecting spatial prominence and symbolic hierarchy embedded in the cultural landscape. High ESV values indicate landmark-like roles, while low values suggest enclosed, introspective spatial character (Lee, 2022; Salerno, 2023).

We used ArcGIS Pro 3.4.0 to extract the values of STWA, STSA, OSV, and ESV based on a DSM-derived spatial model. Afterwards, PCA was conducted to integrate the accessibility and visibility attributes of the CMR into composite spatial characterization indicators for further analysis:

$$A_i = w_1 \cdot STWA_i + w_2 \cdot STSA_i \text{ and } V_i = w_3 \cdot \mathrm{OSV}_i + w_4 \cdot \mathrm{ESV}_i; \tag{1}$$

$$S_i = w_5 \cdot A_i + w_6 \cdot V_i.$$

In Formula (1), where A_i represents the composite accessibility index of scene i; V_i represents the composite visibility index of scene i; S_i represents the composite spatial characterization index of scene i. The PCA weighting factors w_1, w_2, w_3, w_4, w_5, w_6 determine the relative importance of each component. They are derived from the first principal component of each indicator group, using the corresponding explained variance as the weighting coefficient.

2.4.2. Five PHVP scores generated through large language models

In this study, we adopted the few-shot learning approach using Large Language Model (LLM) as proposed by Luo et al. (2025) to analyze the large number of user-generated content. Their comparative study assessed the performance of multiple LLM (Glm/Ernie/Moonshot) in analyzing Chinese user-generated content for cultural perception, while Moonshot-v1 demonstrated superior performance than other similar models in both micro- and macro-averaged precision. Specifically, we utilized the *moonshot-v1-128k* model, incorporating structured prompt engineering inputs that included (1) task instructions, (2) definitions of heritage value categories, (3) background information on CMR, and (4) expert scoring examples for 144 scenes (Table 2).

By embedding these examples into the model prompt, we effectively simulate the decision-making process of human evaluators within a specific context. This structure allows the model to perform controllable dimension-wise scoring under limited supervision by emulating expert evaluation logic embedded in structured prompts.

$$y_i^{(k)} = \sum_{l=1}^{5} \pi_l^{(k)} \cdot I\left[\phi^{(k)}\left(\mathcal{F}_{LLM}\left(c_i \middle| \mathcal{P}_{\text{task}}, \mathcal{P}_{\text{def}}, \mathcal{P}_{\text{bg}}, \mathcal{P}_{\text{ex}}\right)\right) \in R_l\right]. \tag{2}$$

In Formula (2), where $y_i^{(k)}$ is the score for comment c_i on PHVP category k; $\mathcal{F}_{LLM}$ denotes the LLM function guided by structured prompts $\mathcal{P}_{\text{task}}, \mathcal{P}_{\text{def}}, \mathcal{P}_{\text{bg}}, \mathcal{P}_{\text{ex}}$; $\phi^{(k)}(\cdot)$ extracts the semantic content related to PHVP category k ; R_l is the semantic rule for rating level l; $\pi_l^{(k)} = l \in \{1,2,3,4,5\}$ is the corresponding score; and $I\,[\cdot]$ is the indicator function that returns 1 if the model output matches level l, and 0 otherwise.

2.4.3. The perceptual-spatial embeddings for coupling

The two HSCs and the five PHVP scores (Appendix A) were incorporated into the structural embedding framework based on GNN with two-layer graph attention networks as attributes of the nodes (scenes). The connectivity edges among the 144 scenes were constructed using GIS-based OD (Origin-Destination) data in ArcGIS Pro 3.4.0 as the links (KNN). To ensure a meaningful yet computationally efficient network, we applied a classical local neighbourhood coverage criterion, retaining the top-k nearest neighbours with log $n(n = 144) \approx 7$ as the k.

$$\alpha_{ij}^{\mathrm{CMR}} = \frac{\exp\left(\mathrm{LeakyReLU}\left(a^{\top}\left[Wh_i \| Wh_j\right] + \gamma \cdot \mathrm{sim}_{\mathrm{percept}}(i,j)\right)\right)}{\sum_{k \in \mathcal{N}(i)} \exp\left(\mathrm{LeakyReLU}\left(a^{\top}\left[Wh_i \| Wh_k\right] + \gamma \cdot \mathrm{sim}_{\mathrm{percept}}(i,k)\right)\right)}, \tag{3}$$

where $\alpha_{ij}^{\mathrm{CMR}}$ denotes the perception-modulated attention weight from node i to node j. The vectors h_i, $h_j \in R^d$ (with $d = 7$) are the input feature vectors of nodes$i$ and j, comprising two HSCs and five PHVP scores. In the SoftMax denominator, $\mathcal{N}(i)$ iterates over all spatial neighbors of node i and each neighbour k has its own feature vector $h_k \in R^d$. The matrix $W \in R^{d' \times d}$ is a shared learnable linear transformation, producing $Wh_i, Wh_j \in R^{d'}$. The vector $a \in R^{2d'}$ is a trainable attention vector used for computing the attention coefficient via a dot-product with the concatenated input features; $||\cdot||$ denotes concatenation; LeakyReLU is the activation function. The scalar $\gamma > 0$ is a scalar hyperparameter controlling the perceptual similarity and the $\mathrm{sim}_{\mathrm{percept}}(i,j) = \frac{p_i \top \cdot p_j}{\|p_i\| \|p_j\|}$ denotes the perceptual similarity, i.e., the cosine similarity between the normalized five vectors $p_i, p_j \in R^5$ representing the notes i and j. And the neighbour set $\mathcal{N}(i)$ denotes the set of top-$k = 7$ spatial neighbours of node i based on GIS proximity. We set the perceptual similarity weight $\gamma = 0.3$ following prior practices in perceptual attention (Zhou et al., 2024). This value has been demonstrated to be robust in practice, particularly in applications where semantic—structural integration is the primary objective.

In addition, Deep Graph Infomax was employed to encode perceptual-spatial complexity through representation learning to reflect meaningful scene relationships rather than superficial co-occurrences. Following Velickovic et al., 2018, the unsupervised training objective was to maximize mutual information between h_v and s while distinguishing real nodes from corrupted counterparts:

Table 2 The four prompt engineering process of LLM.

Prompt component	Description	Data source/Reference	Function
Task Instructions ($\mathcal{P}_{task}$)	The model was instructed to identify five distinct types of heritage value—historical, cultural, scientific, social, and artistic—reflected in social media comments related to the CMR. Each category was to be rated on a scale from 1 (lowest) to 5 (highest) according to its significance.	This task instruction was adapted from existing research (Luo et al., 2025) and aligns with an expert discussion framework.	Providing clear task instructions can significantly improve the effectiveness of few-shot learning by ensuring the model adheres to a uniform evaluation criterion.
Definition of 5 PHVP ($\mathcal{P}_{def}$)	The PHVP spans five categories: historical (political and ethnic integration), cultural (traditional diversity and synthesis), scientific (site selection and construction techniques), social (education, tourism, religion, and civic life), and artistic (aesthetic landscape and spatial design). (Appendix A. Supp. Mat.1)	Silva and Roders (2012) (UNESCO, 1994) (CHCC and CMACH, 2013)	These definitions served as label explanations or output templates in the few-shot examples, assisting the model in accurately identifying and evaluating each PHVP category. This, in turn, supports targeted comment analysis and enables precise classification and scoring.
Background: Introduction to CMR ($\mathcal{P}_{bg}$)	We indexed 2520 academic articles from the CNKI platform published over the past 30 years related to CMR. Following the basic PRISMA methodology and using abstracts, keywords, and titles, we screened and selected 290 articles with direct relevance. After conducting a literature review, a 3000-character background document was generated.	CNKI	This section clearly establishes CMR as the study subject and, grounded in academic literature, enhances the scientific rigor, credibility, and validity of the overall task.
Expert Scoring Examples for Scenes ($\mathcal{P}_{ex}$)	Relevant documentation for 144 scenes was evaluated by five senior experts across five heritage value categories. Of these, 115 scenes (80 %) were used for model context construction, and 29 scenes (20 %) for testing. The LLM predictions showed strong alignment with expert scores, achieving a Pearson correlation of 0.771, recall of 0.976, and precision of 0.825. The experts—all professor-level senior engineers from the CMR cultural relics team (two from heritage conservation and three from landscape planning), each with over 20 years of experience—ensured the evaluation's credibility.	Collection of historical archives /Expert scoring	This process built a representative labeled dataset that enabled the model to learn diverse and accurate scoring patterns, serving as a reliable reference for the evaluation task. The reserved test set ensured an objective assessment of the model's performance.

$$\mathcal{L}_{PSLPM} = -\sum_{v\in V}\log\sigma\left(\boldsymbol{h}_v^\top\cdot\boldsymbol{s}\right) - \sum_{\tilde{v}\in\tilde{V}}\log\sigma\left(-\boldsymbol{h}_{\tilde{v}}{}^\top\cdot\boldsymbol{s}\right), \tag{4}$$

where corrupted counterparts $\tilde{v}\in\tilde{V}$ denotes a corrupted negative node obtained by randomly shuffling input features, and $\sigma(\cdot)$ is the sigmoid activation function. This contrastive loss encourages the embeddings h_v to align with the overall graph context, which is represented by global context vector s of the entire graph in Deep Graph Infomax. Here, h_v denotes the 32-dimensional embedding of scene v, capturing its perceptual—spatial features by interacting with surrounding structural and semantic patterns. The objective maximizes mutual information between h_v and s, while minimizing the alignment between embeddings of corrupted nodes $\boldsymbol{h}_{\tilde{v}}$ and s, thereby enhancing the context-awareness and robustness of the learned representations.

In terms of coupling, this process yielded 32D embeddings using Graph Attention Networks and Deep Graph Infomax that effectively capture two HSCs and five PHVP (7-dimensional input) for coupling them together. Rather than a merely trivial expansion from this original 7-dimensional input, this transformation served as semantic fusion: reencoding heterogeneous attributes through cross-feature interaction and structural context to reflect scene topology (Ye et al., 2024). Given the weak heterogeneity of the input, higher dimensional embeddings are essential for sufficient representational capacity to capture structural and semantic complexity (Qiang et al., 2025). Prior studies have shown that dimensional expansion enhances representational capacity for knowledge prediction and alignment (Liu et al., 2023; Luo et al., 2021; Tran and Park, 2024). Moreover, appropriate higher dimensional embeddings help to better separate noise and extract latent patterns (Dai et al., 2022; Yu et al., 2023).

In contrast, using the original 7-dimensional data in linear models such as traditional regression, which doesn't fully to capture the sequential effects of heritage-related spatial and perceptual characteristics along visitor trajectories. With 144 nodes representing a moderate-scale network, 32D embeddings provide a widely adopted and empirically supported middle ground, balancing complexity, representational capacity, robustness, and generalization (Cao et al., 2024; K. Wang et al., 2024). For the scale of scenes (nodes) in CMR, lower-dimensional (eg., 16D) embeddings would lack expressive power and struggle to capture interaction structures in weakly heterogeneous data (Gu et al., 2021), while excessively high dimensions—with far more parameters than nodes (e.g., 64D or 128D)—may lead to overfitting (Xu et al., 2023).

The embeddings *h* and *v* were aligned with PHVP through correlation-weighted interpretable reconstruction to ensure semantic coherence, reduce redundancy, and improve interpretability (Liu et al., 2022). Pearson correlation was used to weight and align each embedding with the five PHVP. For each PHVP category *k*, all 32D embeddings were ranked by the absolute correlation with *k*, and categories with Pearson's $r > 0.3$ were selected as its dominant representation dimensions (positively correlated). The selected coupling PHVP (C-PHVP) categories, representing enhanced versions of the original LLM-derived PHVP scores with two embedded HSCs' influences (Pearson's $|r| > 0.3$), both positively and negatively correlated), reflect a common *post hoc attribution* strategy—where GNN embeddings are associated with task-specific variables to identify semantically aligned and interpretable dimensions (Pope et al., 2019; Ying et al., 2019). Using Pearson correlation to align embeddings with the five C-PHVP serves as a targeted attribution method—ensuring task relevance and reducing noise, rather than relying on unsupervised dimensionality reduction. We calculated a perception-weighted C-PHVP score based on the selected embeddings:

$$(C-PHVP\ Score\ Definition)\, s_i^{(k,C-PHVP)} = \sum_{d \in D_k} w_d^{(k)} \cdot z_{i,d},$$
$$\text{with} \quad w_d^{(k)} = \frac{\rho_d^{(k)}}{\sum_{d \in D_k} \left|\rho_d^{(k)}\right|}, \tag{5}$$

where $z_{i,d}$ denotes the value of the *d*-th embeddings for node *i*; $w_d^{(k)}$ is the normalized weight derived from the Pearson correlation between the *d*-th embeddings and the *k*-th PHVP category, restricted to the subset $D_k = \{d \,|\, |\rho_d^{(k)}| > 0.3\}$, when the D_k includes all embedding *d* for which the absolute value of the Pearson correlation coefficient *r* ($\rho_d^{(k)}$) between the *d*-th embedding and *k*-th PHVP category is greater than 0.3; and $s_i^{(k,C-PHVP)}$ represents the final C-PHVP score of node *i* with respect to PHVP category *k*.

2.4.4. The optimized tourism routes and baseline comparison

The final five C-PHVP scores of each scene (node) and the pairwise OD distance matrix were jointly incorporated into a multi-objective evolutionary algorithm (MOEA) framework. We employed the Non-dominated Sorting Genetic Algorithm II to simultaneously optimize for two objectives: maximizing the average five C-PHVP scores and minimizing the total route distance.

To ensure logical and feasible route structures, we imposed classical constraints, including (1) non-repetition of nodes, (2) fixed starting points (entrance and exit), (3) closed-loop route configurations, and (4) a specified tour time (3—7 h) for the route. The algorithm was configured with standard yet context-specific settings: population size = 100, number of generations = 200, crossover probability = 0.9, and mutation probability = 0.05. These values were selected not only based on established evolutionary optimization literature (Deb et al., 2002; Zhang, 2024), but also in consideration of the structural characteristics of the CMR graph—a medium-sized network of 144 nodes with moderate connectivity and high perceptual heterogeneity. This setup ensured sufficient search space coverage and solution diversity, without incurring excessive computational cost.

$$\text{maximize}: F(R) = \left[S^{his}(R), S^{cul}(R), S^{art}(R), S^{sci}(R), S^{soc}(R)\right],$$
$$\text{with } S_k(R) = \frac{1}{|R|}\sum_{v \in R} S_k(v). \tag{6}$$

$$\text{minimize}: D(R) = \sum_{t=1}^{T-1} dist(v_t, v_{t+1}), \tag{7}$$
with $dist(i,j) = D_{ij}$ from distance matrix D.

$$R_{t+1} = \text{Select}(\text{Nondominated-Sort}(R_t \cup \text{Crossover}_{route}(R_t) \cup \text{Mutation}_{PHVP}(R_t))). \tag{8}$$

Subject to the following constraints

$$\begin{cases} (a)\text{Non}-\text{repetition of nodes}: v_i \neq v_j, \forall i \neq j, v_i, v_j \in R, \\ (b)\text{Fixed starting point}: v_1 = v_{\text{entrance and exit}}, \\ (c)\ \text{Closed}-\text{loop path}: v_T = v_1, \\ (d) f_{\text{time}}(R) = \dfrac{D(R)}{4} + \displaystyle\sum_{i=1}^{T} t_{\text{stop}}(v_i) \in [3,7]\ \text{hours}. \end{cases} \tag{9}$$

These three formulas describe the route optimization process based on a multi-objective evolutionary algorithm. In Formula (6), the route $R = [v_1, v_2, ..., v_T]$ represents a sequence of scenes (nodes), and the objective is to maximize the five C-PHVP scores $F(P) = [S^{his}(R), S^{cul}(R), S^{art}(R), S^{sci}(R), S^{soc}(R)]$, where each category score $S_k(R)$ is the average of the corresponding scores of all nodes along the route. Formula (7) aims to minimize the total travel distance $D(R) = \sum_{t=1}^{T-1} dist(v_t, v_{t+1})$, with distances derived from the entries D_{ij} of the distance matrix D. Formula (8) describes the iterative population of candidate routes update process where the current population R_t undergoes route-structure-based $\text{Crossover}_{\text{route}}(R_t)$ and PHVP mutation $\text{Mutation}_{\text{PHVP}}(R_t)$ to generate offspring; these offspring are merged with the current population and then filtered through nondominated sorting *Nondominated-Sort* and *Select* to form the next generation R_{t+1}, achieving a Pareto-optimal balance across multiple objectives. Formula (9) represents the total travel time $f_{\text{time}}(R)$ within 3–7 h includes the walking duration—estimated as *D(R)*/4 based on an average walk speed of 4 km/h—and the cumulative stop time at each node (10 min).

In this study, we established two representative **baselines** to comprehensively evaluate the relative advantages and applicability of our PSLPM routes (PRs). The first baseline is two Official Routes (ORs), namely the two officially recommended routes explicitly displayed on the guide boards at the entrance of CMR. These routes are primarily designed along linear spatial axes and link major landmarks (some scenes), reflecting a managerial logic grounded in spatial structure and connectivity of iconic scenes. The second baseline comprises five theme-based routes generated through a greedy algorithm (GRs), each corresponding to one of the five PHVP. These routes connect the highest-scoring scenes within each PHVP category. This type of route planning exemplifies existing approaches that only focus on preference-driven optimization while overlooking spatial structural balance.

3. Results

3.1. The spatial characterization

We found that within the same scene in the CMR, there are substantial differences between STWA, STSA, ESV, and OSV indicators (Fig. 3[A–D]), articulating these scenes exhibit substantial differences in both visibility and accessibility. The composite accessibility (A_i) was derived by integrating the STWA ($w_1 = 0.532$) and STSA ($w_2 = 0.468$) (Fig. 3[E]), while the first principal component alone accounted for 94.35% of the total variance by PCA. And composite visibility (V_i) was combined with OSV ($w_3 = 0.581$) and ESV ($w_{4.} = 0.419$), while the first principal component explained 89.37% of the total variance (Fig. 3[F]). Furthermore, we applied the natural breaks method to classify all 144 scenes according to A_i (0.549) and V_i (0.268) into four distinct categories (Table 3).

In general, the spatial distribution of the composite spatial index (S_i) across scenes in CMR is notably uneven, which was combined with A_i ($w_5 = 0.508$) and V_i ($w_6 = 0.498$), while the first principal component accounted for 92.19% of the total variance (Fig. 3[G–H]). Scenes classified as Level 1–3, characterized by high accessibility and visibility, are predominantly located in the southeastern lake area. Those with medium values (Level 4–6) are mainly situated in the transitional plains extending from the southeast toward the northern zone. In contrast, scenes within the mountainous areas tend to have lower S_i values and are largely concentrated in Levels 7–9.

3.2. PHVP analysis based on LLM and GNN

Based on four sets of prompts, we derived 1–5 scores for five PHVP categories using LLM. These five PHVP scores

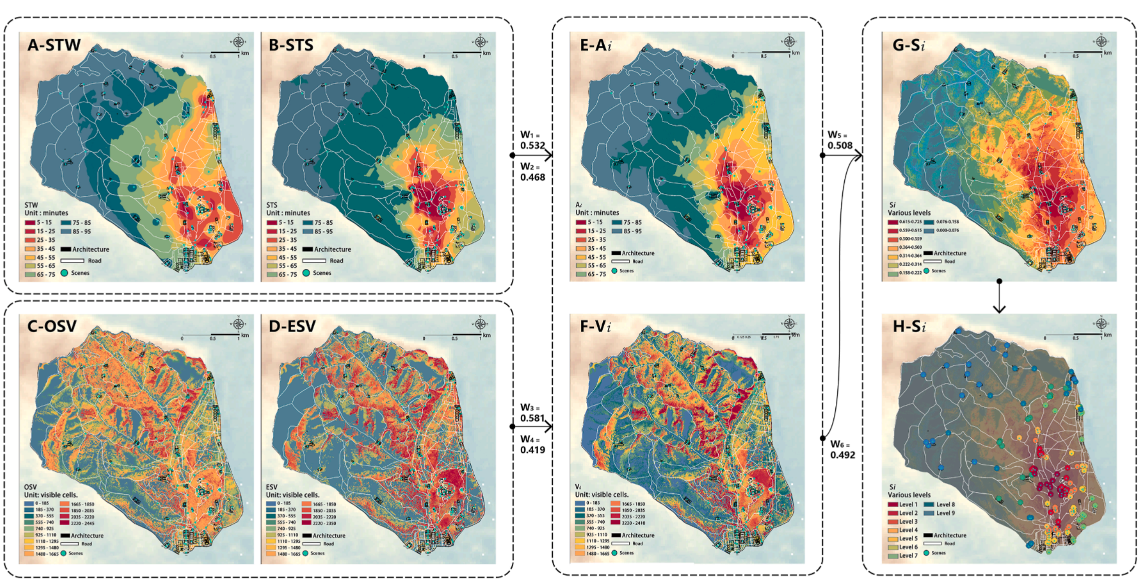

Fig. 3 Both accessibility and visibility were derived through a dimensionality reduction process based on PCA-weighted integration in Formula (1).

Table 3 The four categories of scenes clustered by A_i and V_i.

Category	A_i (Composite accessibility)	V_i (Composite visibility)	No.	Description
HH	High (0.549–1)	High (0.268–1)	62	Scenes with both high A_i and V_i, predominantly located around the southeastern lakes. These include a cluster of scenic and recreational heritage buildings.
HL	High (0.549–1)	Low (0–0.268)	36	Scene characterized by high A_i but limited V_i. This group mainly comprises enclosed historical royal functional structures, such as interior sections of political palaces.
LH	Low (0–0.549)	High (0.268–1)	25	Scenes with low A_i but high V_i, typically situated on elevated terrain in mountainous areas. Most are pavilions intended for viewing the landscape.
LL	Low (0–0.549)	Low (0–0.268)	21	Scenes with both low A_i and low V_i, often located in the western and northern zones, far from the main entrance. These are predominantly religious buildings.

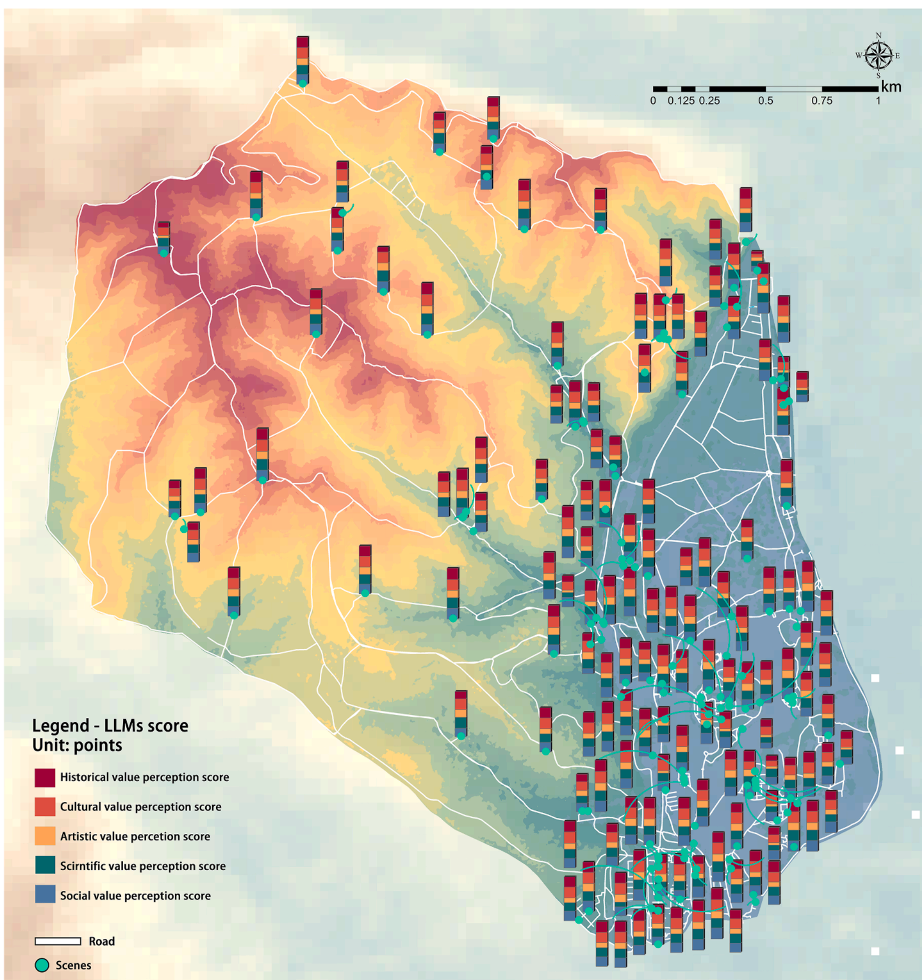

Fig. 4 The spatial-geographical mapping of LLM-generated scores.

were subsequently visualized in a spatial-geographical mapping (Fig. 4). Using a Graph Attention Networks and Deep Graph Infomax system, we conducted 10 iterations of unsupervised learning, resulting in a heatmap of 32D embeddings averaged across all scenes (Fig. 5).

The relationships between the 32D embeddings and the five PHVP categories vary significantly. We visualized their Pearson correlation coefficients and identified the most relevant embeddings of each PHVP category (Pearson's $r > 0.3$, positively correlated) (Fig. 6, Table 4). Their

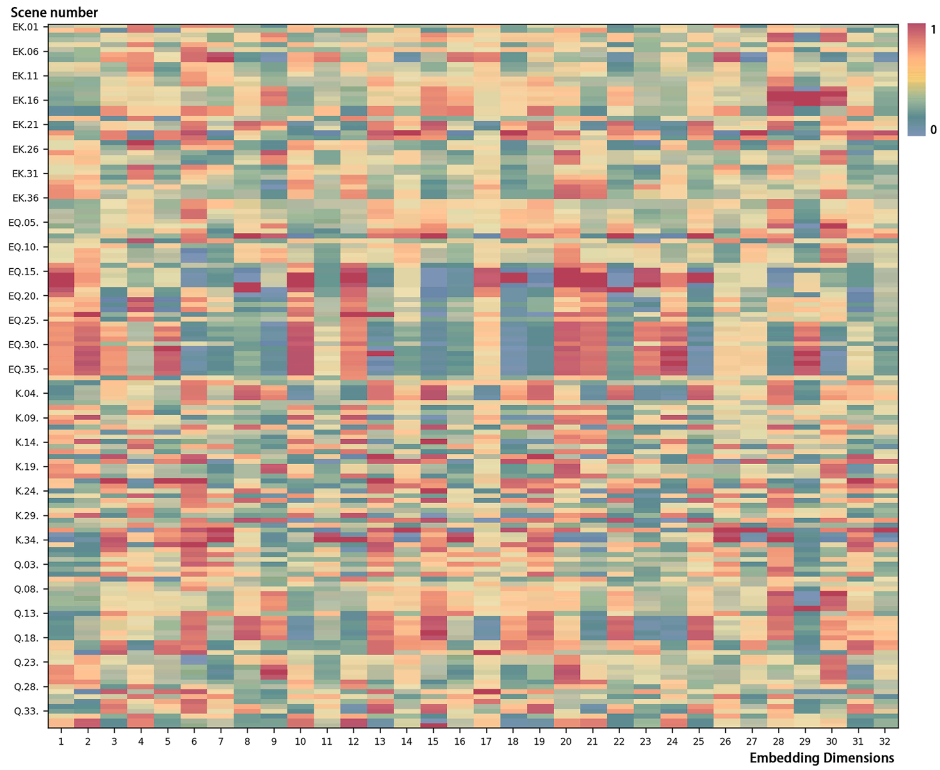

Fig. 5 The heatmap of 32D embeddings averaged across all 144 scenes.

correlations with two HSCs(A_i and V_i) ranged from 0.489 to 0.935 (also Pearson's $|r| > 0.3$, positively and negatively correlated), indicating moderate to robust associations. These were subsequently used in a weighted analysis to derive the final spatial—perceptual C-PHVP scores. To validate the contribution of GNN-based embeddings, we conducted an ablation experiment comparing raw input features (7D) with Graph Attention Networks embeddings of

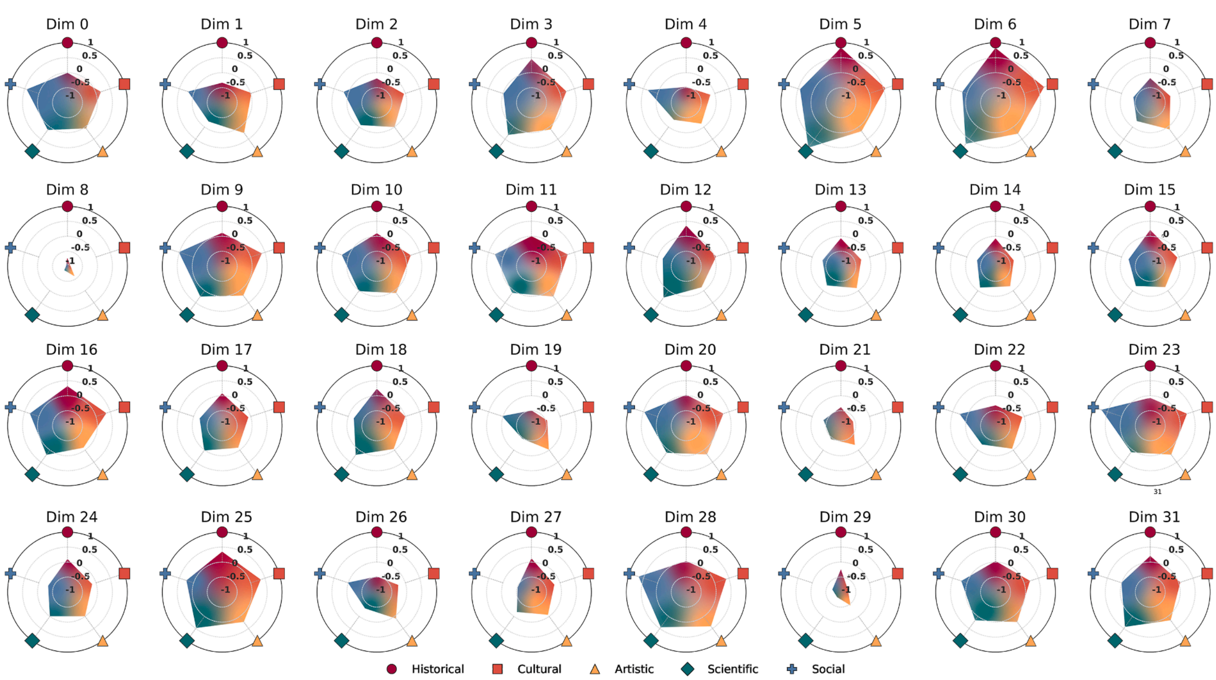

Fig. 6 Pearson correlation coefficients between the 32-dimensional embeddings and the five public heritage value perception categories.

Table 4 Top Pearson correlation coefficients ($r > 0.3$) between the 32D embeddings and five PHVP categories, and their two HSCs index ($|r| > 0.3$).The complete table is provided in Appendix A (Supp. Mat.3).

Dim	Historical value	Cultural value	Artistic value	Scientific value	Social value	A_i	V_i
0	−0.019	0.132	0.036	0.088	[b]0.390	−0.574	−0.490
1	−0.299	0.010	[b]0.326	−0.207	[b]0.307	−0.459	−0.618
3	[b]0.431	0.177	0.073	0.262	−0.026	0.536	−0.513
5	[a]0.819	[a]0.547	0.136	[a]0.827	0.252	0.935	0.857
6	[a]0.807	[a]0.684	[a]0.358	[a]0.671	0.129	0.662	−0.721
9	0.087	[b]0.345	0.159	0.195	[b]0.439	−0.373	−0.547
12	[b]0.335	0.029	−0.127	0.228	−0.168	0.627	0.705
16	0.258	[b]0.344	−0.094	0.152	0.258	−0.764	−0.892
20	0.013	0.246	0.141	0.082	[b]0.426	−0.844	−0.602
23	−0.076	0.231	0.149	0.064	[a]0.555	−0.715	−0.766
25	[b]0.33	0.289	0.181	[b]0.459	0.204	0.611	−0.493
28	0.015	[b]0.34	[a]0.607	0.268	[a]0.541	−0.815	−0.674
30	0.016	0.163	[b]0.313	0.124	0.156	0.489	0.544
31	0.159	0.034	0.122	[b]0.412	−0.005	0.506	0.486

[a] Indicates strong correlation, with $r > 0.5$.
[b] Indicates moderate correlation, with $r > 0.3$.

varying dimensions (16D, 32D, 64D) (Table 5). The 32D embedding achieved the highest average perceptual score (0.723), the lowest perceptual variance (0.089), and a reasonable computational cost. These results support the choice of 32D as the main configuration, balancing semantic expressiveness and perceptual stability.

3.3. Thematic and multi-layered route design

We obtained the final perceptual-spatial C-PHVP scores for all 144 scenes (Appendix A, Supp. Mat.4), along with their spatial connectivity attributes derived from GIS. After the MOEA process, five PSLPM distinct route outputs were obtained each emphasizing a specific theme (Fig. 7, Table 6). For each theme, both long-route and short-route variants were generated. Meanwhile, many scenes exhibit high composite indicators and thus play multiple roles. We grouped these into a composite route.

3.4. Comparative research of two baselines

3.4.1. Comparative analysis of HSCs

The A_i and V_i values across different scenes reflect distinct spatial characteristics. In Section 3.1, we clustered the scenes into four categories: HH, HL, LH, and LL based on

Table 5 Model input settings and performance comparison on PHVP tasks.

Feature setting	Feature type	Dimension	Avg. PHVP	Std. Dev. (diversity)	Runtime (s) NVIDIA RTX 3090	Explanation
Raw input (baseline)	2 HSCs+ 5PHVP scores	7	0.445	0.125	24.3	No GNN semantic fusion; insufficient alignment with PHVP
Graph Attention Networks + Deep Graph Infomax embedding	GNN-based embedding	16	0.571	0.114	35.2	Lower expressive power; Embedding too shallow; limited perceptual generalization
Graph Attention Networks + Deep Graph Infomax embedding	GNN-based embedding	[a]32	[a]0.723	[a]0.089	[a]37.8	Best trade-off between value expression, balance, and cost
Graph Attention Networks + Deep Graph Infomax embedding	GNN-based embedding	64	0.684	0.127	45.9	Overfitting risk; Marginal gain in value, but increased noise and cost

[a] Indicates the optimal setting across all evaluation metrics.

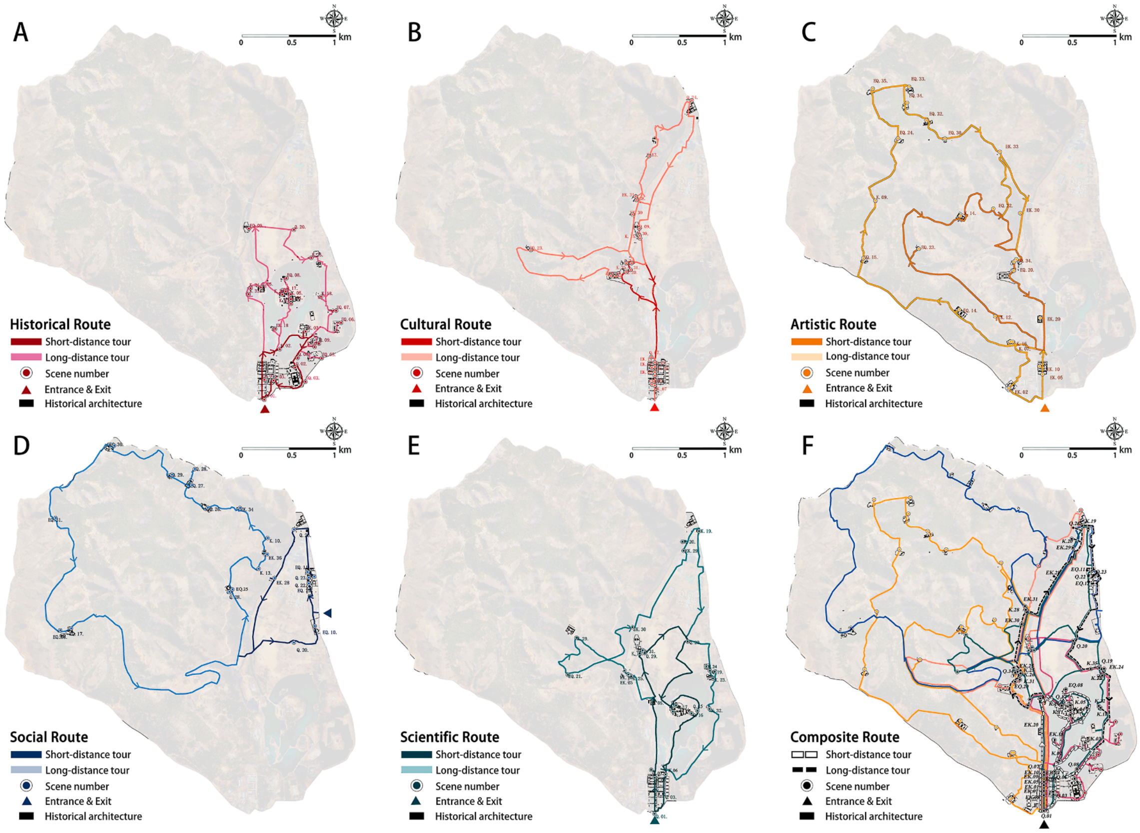

Fig. 7 The five PSLPM routes and a composite route generated from MOEA.

Table 6 The attributes of five thematic routes and a composite route.

Theme route	Number of scenes	Historical scores	Cultural scores	Artistic scores	Scientific scores	Social scores	Short tour distance (m)	Long tour distance (m)
Historical route	28	[a]0.720	0.389	0.267	0.542	0.437	2051.15	4278.34
Cultural route	22	0.599	[a]0.758	0.641	0.562	0.537	2975.19	4193.37
Artistic route	24	0.361	0.663	[a]0.784	0.493	0.573	3192.46	5496.07
Scientific route	27	0.539	0.495	0.514	[a]0.672	0.375	3218.83	5016.97
Social route	22	0.360	0.459	0.576	0.224	[a]0.682	2933.43	9739.704
Composite route	49	0.565	0.457	0.665	0.559	0.532	3640.244	4090.95

[a] Indicates the highest perception score among all routes in the corresponding category.

these indicators. The PRs, Ors and GRs exhibit divergent distributions across these spatial clusters (Table 7). And we also calculate the distribution of PRs, Ors, and GRs across spatial 1–9 levels based on S_i (Table 8).

Across all thematic categories, the PRs cover all four spatial types, with HH areas accounting for 32%–59.26%, HL for 24%–36.36%, LH for 3.45%–24%, and LL for 3.45%–20%. The route lengths range from 6.329 to 12.673 km, reflecting considerable spatial diversity and a relatively balanced spatial structural distribution. In contrast, the GRs also prioritize HH areas (50%–67%), but show no coverage of LL nodes. Some themes exhibit extreme concentrations in LH areas (e.g., 100% for the social theme), and the overall route lengths are significantly longer (14.536–21.053 km). The ORs (OR1 and OR2) are mainly concentrated in HH and HL zones (with HH proportions of 56% and 62.07%, and HL proportions of 44% and 37.93%, respectively), entirely lacking LH and LL nodes. Their distances are 10.508 km and 12.120 km, indicating a more spatially centralized pattern.

3.4.2. Comparative analysis of PHVP

The violin plots illustrate clear distinctions among the three route types—PRs, GRs, and ORs—in terms of five PHVP (Fig. 8). Overall, GRs consistently exhibit the highest mean scores across all categories, with particularly notable values in the artistic (0.883), scientific (0.866), and social (0.898) categories. These high scores are accompanied by relatively low standard deviations (0.055, 0.052, and 0.077), indicating a strong concentration on high-perception nodes and internal consistency. PRs demonstrate moderate scores across the five dimensions—historical (0.739), cultural (0.682), artistic

Table 7 Distribution of PRs, ORs, and GRs across spatial categories (HH, HL, LH, LL) based on A_i and V_i.

Theme route/ (A_i & V_i categories)	Historical category		Cultural category		Artistic category		Scientific category		Social category		ORs	
	PR	GR	PR	GR	PR	GR	PR	GR	PR	GR	OR1	OR2
HH (%)	58.62	56.56	45.45	50.00	24.00	50.00	59.26	67.00	18.18	*0.00	56.00	62.07
HL (%)	31.3	22.22	36.36	50.00	24.00	*0.00	25.93	22.00	4.55	*0.00	44.00	37.93
LH (%)	3.45	22.22	9.09	*0.00	20.00	50.00	7.41	11.00	40.91	100.00	*0.00	*0.00
LL (%)	3.45	*0.00	9.09	*0.00	32.00	*0.00	7.41	*0.00	36.36	*0.00	*0.00	*0.00
Distance (km)	6.32	15.50	7.168	14.53	8.688	18.019	8.235	14.793	12.673	21.053	10.508	12.12

The * indicates an extreme or boundary value (typically 0.00) within the column, highlighting the absence or exclusivity of a specific perceptual—spatial category under the given route.

Table 8 Distribution of PRs and ORs across spatial levels based on S_i.

Theme route (S_i)	Level 1	Level 2	Level 3	Level 4	Level 5	Level 6	Level 7	Level 8	Level 9
PRs	7.84	12.75	8.82	8.82	12.75	12.75	12.75	10.78	12.75
GRs	6.25	6.25	18.75	18.75	25.00	6.25	6.25	12.50	*0.00
OR1	4.00	24.00	16.00	16.00	36.00	4.00	*0.00	*0.00	*0.00
OR2	6.86	24.14	13.79	13.79	31.03	10.34	*0.00	*0.00	*0.00

The * indicates an extreme or boundary value (typically 0.00) within the column, highlighting the absence or exclusivity of a specific perceptual—spatial category under the given route.

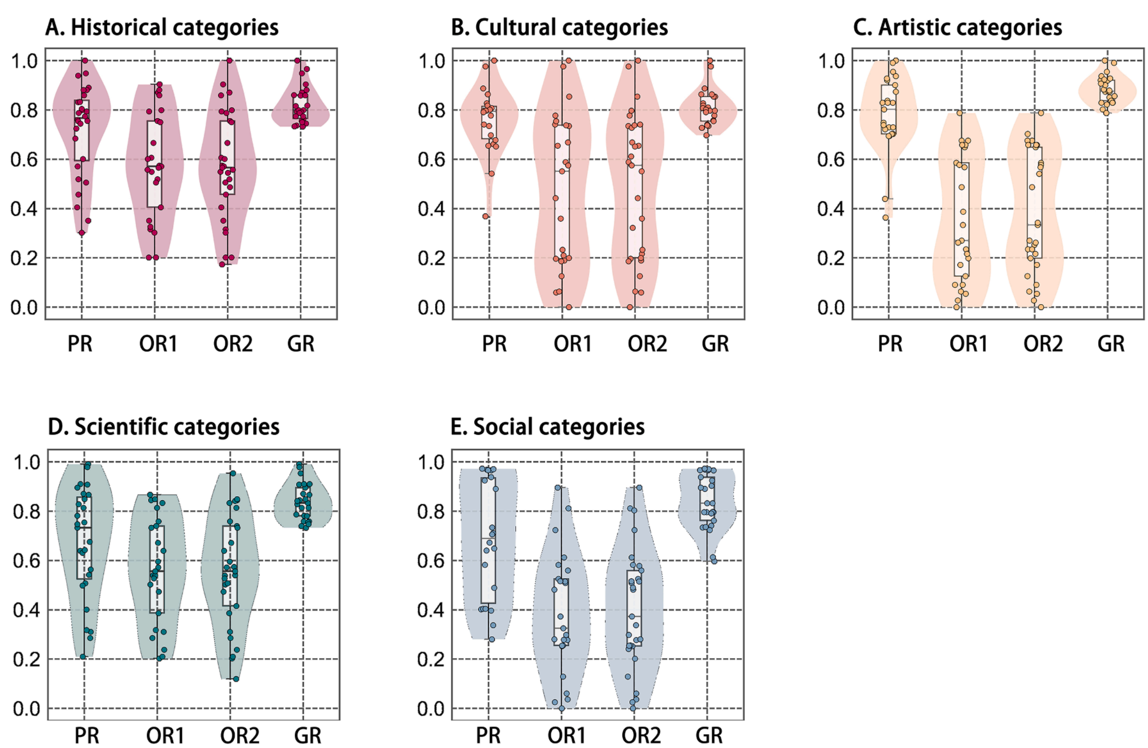

Fig. 8 The distribution of perception scores across five categories for the PRs, OR1, and OR2.

(0.784), scientific (0.783), and social (0.688). The standard deviations for PRs are generally higher than those of GRs but lower than those of ORs, reflecting an approach that emphasizes perceptual-spatial equilibrium by integrating a wider range of spatial levels and combination types. ORs perform the lowest across all categories, with particularly poor outcomes in the artistic (0.37), social (0.427), and cultural (0.484) categories. The standard deviations are also relatively large—for instance, 0.248 in artistic and 0.271 in social—indicating substantial variability in route quality and a lack of perceptual coherence.

3.4.3. Comprehensive comparative analysis

Using the historical-themed route as an example, we included all scenes from the PR, GR, and OR routes to construct spatial image collages. The horizontal axis represents the distance of each scene from the entrance as well as the distances between scenes, while the vertical axis indicates the normalized C-PHVP scores. Colours denote different spatial categories. This visualization reveals the overall PHVP level of each route, along with the extent of coverage and richness of variation across the four spatial types (Fig. 9).

4. Discussion

4.1. Practical reflection from PSLPM

This study proposes the PSLPM as a systematic response to a long-standing issue in cultural landscape practice: the gap between HSCs and PHVP. Such misalignment not only weakens the cultural carrying capacity of landscapes under rapid urbanization but also creates a disconnect between heritage spatial governance and public experience (Qi et al., 2022). As a result, sites with rich cultural connotations but inconspicuous spatial structures are often marginalized, undermining the cultural landscapes' integrity, continuity and sustainability (Khalaf, 2019).

Compared with GRs and ORs, PSLPM couples spatial accessibility and visibility in HSCs with PHVP to generate PRs that exhibit greater structural penetration, spatial diversity, and balanced layout. These PRs encompass a broader range of HSC-defined areas while maintaining high levels of perceived value, effectively avoiding the spatial bias seen in GRs and ORs that tend to overconcentrate on perceptual hotspots or visually dominant nodes. Such biases exacerbate congestion in core areas and diminish opportunities for cognitive engagement with marginalized scenes (both low accessibility and visibility), ultimately impeding comprehensive heritage value communication. The lengths of PRs are also constrained within a practical range, ensuring accessibility while enhancing perceptual engagement. This spatial pattern not only improves visitor mobility experience but also reactivates the cultural potential of marginalized zones, reinforcing the narrative coherence of cultural landscapes and offering a supportive reference for developing more inclusive intelligent navigation systems.

More importantly, PSLPM's construction relies on standardized spatial indicators and modular perception scoring mechanisms, giving the model strong contextual transferability. It is not bound to any specific cultural landscape typology. By simply adapting the source corpus and perceptual dimensions to local heritage contexts, PSLPM can be applied across diverse route optimization practices, where previous research has primarily emphasized circulation efficiency or expert-driven, single-objective linear planning such as historical districts and industrial heritage sites (Balcan et al., 2024; Pei et al., 2022). In addition, PSLPM offers a unified yet flexible analytical framework for communicating cultural values under varying spatial conditions, thereby expanding the theoretical and methodological boundaries of global cultural landscapes' planning practice.

4.2. Theoretical implications of PSLPM

Current studies of cultural landscapes in urban environments have largely consolidated around a perceptual—spatial duality, as reflected in the interdisciplinary studies across human geography, environmental psychology, urban perception theory, and governance research (Bornioli et al., 2023; Singh et al., 2023; Soyer and Tunca, 2025; Liu et al., 2022). Frameworks such as UNESCO's *Historic Urban Landscape* emphasize their role as spatial carriers of urban public memory and identity, while the *European Landscape Convention* stresses individual perception, place attachment, embodied experience of cultural landscapes. However, when the theoretical framework was applied into practice, a persistent disconnection remains between spatial models and perceptual meanings. (Qi et al., 2022; Jamhawi et al., 2023; Zhang et al., 2023; Liu et al., 2022). To fill this gap, we draw upon landscape planning as an interdisciplinary integrative approach that aligns cultural landscape physical structures

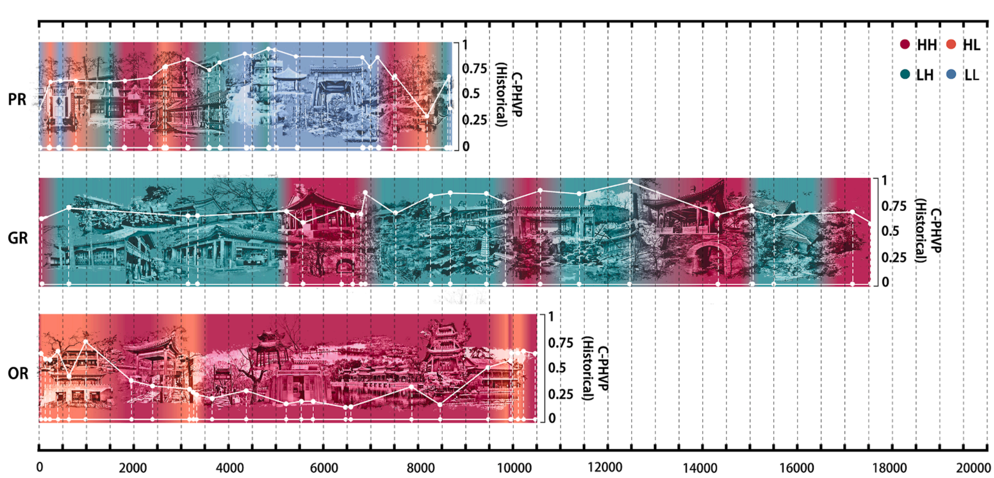

Fig. 9 Comparative distribution of spatial categories and historical C-PHVP scores AlongPR, GR, and OR.

with the intangible public perception (Lian et al., 2024; Ryan, 2011; Sánchez et al., 2020). Building on this foundation, we introduce the PSLPM route optimization as an intervention that utilizes recent advances in social media—based semantic mining and AI-driven perception modeling to deepen the integrative coupling between spatial structure and perceptual meaning.

Methodologically, the study lays the foundation for perceptual computing and the advancement of urban spatial intelligence for cultural landscape planning and management. By embedding semantically derived scores from LLM into GNN structures, PSLPM demonstrates how distributed perceptual data can be translated into structurally expressive embeddings, thereby enhancing the interpretability of high-dimensional spatial representations (Luo et al., 2025; Liu et al., 2022; Pope et al., 2019). While not fully resolving the black-box nature of GNNs, the proposed correlation-based attribution mechanism offers an interpretable interface that links latent graph representations with domain-specific semantic dimensions, providing a replicable, transparent, and generalizable template for explainable spatial intelligence (Z. Liu et al., 2022; Ying et al., 2019). Building on this, PSLPM advances a MOEA that balances spatial diversity, perceptual equity, and experiential coherence (Deb et al., 2002; Zhang, 2024), transcending prior models that rely solely on spatial hierarchy or perceptual hotspots (Smith, 2023; Von Haaren, 2002). This approach supports perceptual value-informed landscape planning and responds to the governance and management challenges of cultural landscapes under the pressure from urban environments.

4.3. Limitations

First, *Mountain Resort and its Outlying Temples, Chengde* was included on UNESCO's World Cultural Heritage list in 1994. However, considering the limitations of available data and spatial constraints, our research primarily focuses on the core part of the heritage site, namely the Chengde Mountain Resort (CMR).

Although this study constructs a multidimensional perception scoring system based on user-generated content, effectively capturing public value perception comments in real-world contexts, certain limitations related to data source bias remain. User-generated content collected is subject to platform recommendation algorithms and the composition of user groups, which may lead to the underrepresentation of specific value types—such as historical or religious significance—due to lower expression frequency or stylistic divergence.

In addition, while weighted-correlation was used to enhance the post hoc interpretability of GNN embeddings, the model still exhibits inherent *black-box* characteristics. Therefore, the newly planned routes need to be checked and evaluated by local administrators and experts. Furthermore, the current modeling assumes relatively stable landscape structures and perception patterns over time, without accounting for dynamic contextual shifts such as real-time tracking of newly planned routes as feedback, aiming for further improvements and simulation studies. This may limit the model's applicability in scenarios involving real-time navigation, adaptive management, or personalized recommendation.

5. Conclusion

PSLPM fundamentally enhances cultural landscape route optimization by transcending purely technical approaches. Through the integration of LLM and GNN, it establishes a value-informed spatial strategy that explicitly bridges the gap between objective HSCs and subjective PHVP. This coupling ensures that experiential sequencing aligns with collective cultural perception. Built upon standardized spatial indicators (accessibility, visibility) and a modular perception scoring mechanism (adaptable LLM prompts for different PHVP dimensions), PSLPM exhibits strong transferability. It can be adapted to diverse cultural landscape typologies by tailoring the source corpus and perceptual categories to local heritage contexts.

For landscape planning managers and heritage governance, PSLPM provides a powerful, data-driven tool sensitive to public perception. It supports strategic objectives such as rebalancing visitor flows to alleviate congestion; enabling more inclusive landscape interpretation by highlighting marginalized areas; informing the development of intelligent navigation systems; and mediating between the inherent spatial logic of landscapes and evolving public cultural meanings. Integration into planning workflows, participatory processes, or smart tourism platforms facilitates more equitable, perceptually resonant, and sustainable cultural landscape development. Thus, PSLPM effectively bridges the persistent gap between spatial structure and perceptual significance, offering a robust pathway for enhancing the cultural landscapes within contemporary urban environments.

Declaration of competing interest

This manuscript is original, has not been published, and is not under consideration elsewhere. All authors have approved the submission and declare that they have no known competing financial interests or personal relationships that could have appeared to influence the work reported in this paper. All authors have approved the submission and declare no conflicts of interest.

Appendix A. Supplementary data

Supplementary data to this article can be found online at https://doi.org/10.1016/j.foar.2025.10.004.

References

Ai, Z., Chiu, D.K.W., Ho, K.K.W., 2024. Social media analytics of user evaluation for innovative digital cultural and creative products: experiences regarding Dunhuang cultural heritage. J. Comput. Cult. Herit. 17 (3), 1—25.

Bai, N., Nourian, P., Luo, R., Cheng, T., Roders, A.P., 2023. Screening the stones of Venice: mapping social perceptions of cultural significance through graph-based semi-supervised

classification. ISPRS J. Photogrammetry Remote Sens. 203, 135—164.
Balcan, C., Aydın, E.Ö., Ünsal, Ö., 2024. Value-based optimization model for cultural route design: Ancient Water Supply Heritage of Istanbul (Türkiye). J. Cult. Herit. 70, 97—110.
Bohnet, I.C., Molnarova, K.J., Van Den Brink, A., Beilin, R., Sklenicka, P., 2022. How cultural heritage can support sustainable landscape development: the case of Třeboň Basin, Czech Republic. Landsc. Urban Plann. 226, 104492.
Bornioli, A., Birenboim, A., Druez, E., Livny, O., Van Der Noll, J., Mayer, N., Bloom, P.B., 2023. Environmental appraisals in outgroup cultural landscapes: the role of Muslim elements in urban settings. Cities 143, 104579.
Cao, J., Fang, J., Meng, Z., Liang, S., 2024. Knowledge graph embedding: a survey from the perspective of representation spaces. ACM Comput. Surv. 56 (6), 1—42.
CHCC&CMACH, 2023. Special conservation plan for the ancient architectural ruins of Chengde Mountain Resort. In: 1C. H. C. C. C. C. M. A. o. C. H. (CMACH). Tsinghua Urban Planning & Design Institute, Beijing.
Dai, E., Jin, W., Liu, H., Wang, S., 2022. Towards robust graph neural networks for noisy graphs with sparse labels. In: Proceedings of the Fifteenth ACM International Conference on Web Search and Data Mining, pp. 181—191.
Deb, K., Pratap, A., Agarwal, S., Meyarivan, T., 2002. A fast and elitist multiobjective genetic algorithm: NSGA-II. IEEE Trans. Evol. Comput. 6 (2), 182—197.
Domingo, I., Smith, C., Jackson, G., Roman, D., 2020. Hidden sites, hidden images, hidden meanings: does the location and visibility of motifsand sites correlate to restricted or open access? J. Archaeol. Method Theor 27 (3), 699—722.
Ducci, M., Janssen, R., Burgers, G., Rotondo, F., 2023. Co-design workshops for cultural landscape planning. Landsc. Res. 48 (7), 900—916.
Gu, W., Tandon, A., Ahn, Y., Radicchi, F., 2021. Principled approach to the selection of the embedding dimension of networks. Nat. Commun. 12 (1), 3772.
Henning, M., Herrmann, P., Zimmermann, T., Meier, M., Pietsch, M., Schmidt, C., 2021. A scenario and monitoring based planning approach to strengthen the resilience of the cultural landscape. J. Digit. Landsc. Architect. 6, 123—132.
Jamhawi, M.M., Zidan, R.J., Sherzad, M.F., 2023. Tourist movement patterns and the effects of spatial configuration in a cultural heritage and urban destination: the case of Madaba, Jordan. Sustainability 15 (2), 1710.
Khalaf, R.W., 2019. Continuity: a fundamental yet overlooked concept in World Heritage policy and practice. Int. J. Cult. Pol. 27 (1), 102—116.
Kim, H., Bone, C., Lee, G., 2020. Landscapes shared by visibility: a case study on the settlement relationships of the Songgukri culture, Korea. Archaeol. Anthropol. Sci. 12 (2), 42.
Lee, J., 2022. Zoning scenic areas of heritage sites using visibility analysis: the case of Zhengding, China. J. Asian Architect. Build Eng. 22 (1), 1—13.
Lian, J., Nijhuis, S., Bracken, G., Wu, X., Wu, X., Chen, D., 2024. Conservation and development of the historic garden in a landscape context: a systematic literature review. Landsc. Urban Plann. 246, 105027.
Liang, K., Liu, H., Shan, M., Zhao, J., Li, X., Zhou, L., 2024. Enhancing scenic recommendation and tour route personalization in tourism using UGC text mining. Appl. Intell. 54 (1), 1063—1098.
Liao, Z., Liang, S., 2025. Spatial pattern of attractiveness and road network accessibility of scenic spots in Guangdong Province based on network information. Sci. Rep. 15, 7950.
Lin, X., Shen, Z., Teng, X., Mao, Q., 2024. Cultural routes as cultural tourism products for heritage conservation and regional development: a systematic review. Heritage 7 (5), 2399—2425.
Liu, Z., Wang, Y., Bernard, J., Munzner, T., 2022. Visualizing graph neural networks with CorGIE: corresponding a *graph* to its embedding. IEEE Trans. Visual. Comput. Graph. 28 (6), 2500—2516.
Liu, Z., Yang, J., Zhong, X., Wang, W., Chen, H., Chang, Y., 2023. A novel composite Graph neural network. IEEE Transact. Neural Networks Learn. Syst. 35 (10), 13411—13425.
Liu, J., Zhang, M., Xia, Y., Zheng, H., Chen, C., 2022. Using agent-based modeling to assess multiple strategy options and trade-offs for the sustainable urbanization of cultural landscapes: a case in Nansha, China. Landsc. Urban Plann. 228, 104555.
Liu, H., Zheng, C., Li, D., Zhang, Z., Lin, K., Shen, X., Xiong, N.N., Wang, J., 2022. Multi-perspective social recommendation method with graph representation learning. Neurocomputing 468, 469—481.
Luo, G., Li, J., Su, J., Peng, H., Yang, C., Sun, L., Yu, P.S., He, L., 2021. Graph entropy guided node embedding dimension *selection* for graph neural networks. arXiv preprint arXiv:2105.03178.
Luo, H., Zhang, Z., Zhu, Q., Ameur, N.E.H.B., Liu, X., Ding, F., Cai, Y., 2025. Using large language models to *investigate* cultural ecosystem services perceptions: a few-shot and prompt method. Landsc. Urban Plann. 258, 105323.
Öztürk, S.Ç., Aktan, E.Ö.A., 2024. A cultural route recommendation based on optimization techniques in urban spaces. Int. J. Sustain. Dev. Plann. 19 (9), 3417—3430.
Pei, Q., Wang, L., Du, P., Wang, Z., 2022. Optimization of tourism routes in Lushunkou District based on ArcGIS. PLoS One 17 (3), e0264526.
Pope, P.E., Kolouri, S., Rostami, M., Martin, C.E., Hoffmann, H., 2019. Explainability methods for graph convolutional neural networks. In: 2022 IEEE/CVF Conference on Computer Vision and Pattern Recognition (CVPR), pp. 10764—10773. Long Beach, CA, USA, 2019.
Qi, J., Zhou, Y., Zeng, L., Tang, X., 2022. Aesthetic heterogeneity on rural landscape: pathway discrepancy between perception and cognition. J. Rural Stud. 92, 383—394.
Qiang, B., Liu, T., Du, P., Li, P., Wang, W., Xu, S., 2025. Drainage pattern recognition method using graph convolutional networks combined with Three-Dimensional Elevation features. Trans. GIS 29, e70002.
Ryan, C., 2020. Advanced Introduction to Tourism Destination Management. Edward Elgar Publishing.
Ryan, R.L., 2011. The social landscape of planning: integrating social and perceptual research with spatial planning information. Landsc. Urban Plann. 100 (4), 361—363.
Sahle, M., Saito, O., 2021. Mapping and characterizing the Jefoure roads that have cultural heritage values in the Gurage socio-ecological production landscape of Ethiopia. Landsc. Urban Plann. 210, 104078.
Salerno, R., 2023. Representation and visualization processes for a sustainable approach to Landscape/Heritage. Sustainability 15 (19), 14589.
Sánchez, M.L., Cabrera, A.T., Del Pulgar, M.L.G., 2020. Guidelines from the heritage field for the integration of landscape and heritage planning: a systematic literature review. Landsc. Urban Plann. 204, 103931.
Silva, A.T.P., Roders, A.P., 2012. Cultural heritage management and heritage (impact) assessments. In: Proceedings of the Joint CIB W070, W092 & TG72 International Conference on Facilities Management, Procurement Systems and Public Private Partnership, 23-25 January 2012, Cape Town, South Africa.
Singh, R.P.B., Niglio, O., Rana, P.S., 2023. Interfaces among placemaking and cultural landscapes: review and appraisal. In:

Singh, R.P.B., Niglio, O., Rana, P.S. (Eds.), Placemaking and Cultural Landscapes. Advances in Geographical and Environmental Sciences. Springer, Singapore, pp. 3—21.

Smith, J., 2023. Conserving cultural landscapes. In: Cameron, C. (Ed.), Evolving Heritage Conservation Practice in the 21st Century. Springer Nature, Singapore, pp. 97—112.

Soyer, F., Tunca, E.A., 2025. Political and cultural memory in urban space: public naming practices in Northern Cyprus. Cities 160, 105851.

Tena, P.A., Sánchez, X.G., Vicente, V.a.Q., García-Esparza, J.A., 2024. Unpacking World Heritage cultural clusters through the interplay of urban tourism and gentrification. Cities 158, 105634.

Tran, D., Park, M., 2024. FN-GNN: a novel graph embedding approach for enhancing graph neural networks in network intrusion detection systems. Appl. Sci. 14 (16), 6932.

Trichopoulos, G., 2023. Large language models for cultural heritage. In: Proceedings of the 2nd International Conference of the ACM Greek SIGCHI Chapter, pp. 1—5. Article 33.

UNESCO, 1994. Inscription: the Mountain resort and its outlying temples, chengde (China). S. a. C. O. United Nations Educational.

Vansteenwegen, P., Souffriau, W., Van Oudheusden, D., 2010. The orienteering problem: a survey. Eur. J. Oper. Res. 209 (1), 1—10.

Velickovic, P., Cucurull, G., Casanova, A., Romero, A., Liò, P., Bengio, Y., 2018. Graph attention networks. arXiv (Cornell University). https://doi.org/10.17863/cam.48429.

Von Haaren, C., 2002. Landscape planning facing the challenge of the development of cultural landscapes. Landsc. Urban Plann. 60 (2), 73—80.

Wallach, B., 2005. Understanding the Cultural Landscape. Guilford Press.

Wang, B., Dane, G., De Vries, B., Arentze, T., 2024. Design and test of a multi-Media Web Platform *prototype* based on people's preferences to increase cultural heritage awareness. Sustainability 16 (22), 10065.

Wang, K., Lin, D., Luo, S., 2024. Graph percolation embeddings for efficient knowledge graph reasoning. IEEE Trans. Knowl. Data Eng. 37 (3), 1198—1212.

Wong, I.A., Lian, Q.L., Sun, D., 2023. Autonomous travel decision-making: an early glimpse into *ChatGPT* and generative AI. J. Hospit. Tourism Manag. 56, 253—263.

Wu, X., Chen, C., 2022. Spatial distribution and accessibility of high level scenic spots in Inner Mongolia. Sustainability 14 (12), 7329.

Xu, Q., Xu, Y., Ma, C., 2024. Analysis of contemporary value and influence of intangible cultural heritage based on online review mining. PLoS One 19 (12), e0315805.

Xu, X., Ding, Z., Wu, Y., Yan, J., Jiang, S., Cui, Q., 2023. Optimal node embedding dimension selection using overall entropy. In: Lecture Notes in Computer Science, pp. 114—127.

Ye, M., Yu, Y., Shen, Z., Yu, W., Zeng, Q., 2024. Cross-feature interactive tabular data modeling with multiplex graph neural networks. IEEE Trans. Knowl. Data Eng. 36 (12), 7851—7864.

Ying, Z., Bourgeois, D., You, J., Zitnik, M., Leskovec, J., 2019. Gnnexplainer: generating explanations for graph neural networks. Adv. Neural Inf. Process. Syst. 32.

Yu, Z., Zhang, C., Deng, C., 2023. An improved GNN using dynamic graph embedding mechanism: a novel end-to-end framework for rolling bearing fault diagnosis under variable working conditions. Mech. Syst. Signal Process. 200, 110534.

Zhang, B., Zhou, L., Yin, Z., Zhou, A., Li, J., 2023. Study on the correlation characteristics between scenic byway network accessibility and self-driving tourism spatial behavior in Western Sichuan. Sustainability 15 (19), 14167.

Zhang, F., 2024. Constructing a multi-objective optimization model for engineering projects based on NSGA-II Algorithm under the background of green construction. Decision Making Appl. Manage. Eng. 7 (1), 37—53.

Zhang, R., Taylor, K., 2020. Cultural landscape meanings. The case of West Lake, Hangzhou, China. Landsc. Res. 45 (2), 164—178.

Zhou, Z., Shi, J., Zhang, H., Chen, Q., Wang, X., Chen, H., Wang, Y., 2024. CreST: a credible spatiotemporal learning framework for uncertainty-aware traffic forecasting. In: *In Proceedings of the 17th ACM* International *Conference on Web Search and Data Mining*, pp. 985—993, 985—993.